

(IRS) to enhance an orthogonal frequency division multiplexing (OFDM) based ISAC system, ensuring the communication rate of the desired user was maintained. The authors in Ref. [6] investigated the robust beamforming design under the statistical CSI, focusing on SINR requirements. They proposed a double-loop deep unfolding (DU) approach to address this challenge, and simulation results underscored the effectiveness of their proposed robust beamforming design algorithm. From the sensing perspective, the authors in Ref. [7] proposed a robust beamforming scheme by adopting the CRB for angle estimation as the sensing performance metric, and the simulation results demonstrated that the proposed scheme maintained robust direction of arrival (DoA) estimation performance across various targets, indicating its effectiveness. As a step further, the authors in Ref. [8] explored the impact of reconfigurable intelligent surfaces (RIS) in mitigating multi-user interference (MUI) while satisfying CRB constraints. Their simulation results demonstrated superior estimation performance compared with previous works based on SINR of echo signals. The authors in Ref. [9] focused on sidelobe control in sensing to enhance target detection performance. Additionally, authors in Ref. [10] investigated the detection probability in radar sensing with binary detection, incorporating Minorize-Maximize (MM) algorithms to achieve optimal sensing beam-patterns across diverse scenarios.

It can be seen that the aforementioned existing work utilizes different metrics for sensing and communication to achieve the performance tradeoff in ISAC systems. In the absence of a unified metric for ISAC system design, the authors in Refs. [11] and [12] employed mutual information (MI) to evaluate the performance of communication and sensing. Simulation results showed MI could be used to assess the efficiency of transmission and achieve the performance tradeoff in ISAC systems. From the perspective of detection, the authors in Refs. [13] and [14] respectively employed Kullback-Leibler (KL) divergence to analyze ISAC systems, thereby formulating a unified design framework. Furthermore, the authors in Ref. [15] proposed a novel allocation approach to ISAC systems using KLD. Simulation results demonstrated that the proposed scheme achieved a higher KLD compared with the uniform power allocation scheme. These approaches provide a comprehensive method to balance and optimize both sensing and communication functionalities within ISAC systems. However, all the above studies overlook the interference caused by clutter in the environment, potentially degrading the sensing performance in realistic ISAC systems.

In this paper, we employ KLD as a unified performance metric to design ISAC systems and construct a model that accounts for the presence of static clutter for ISAC scenarios. In particular, we focus on constellation and beamforming design with the aim of investigating the performance tradeoff and achieving clutter suppression. A successive convex approxima-

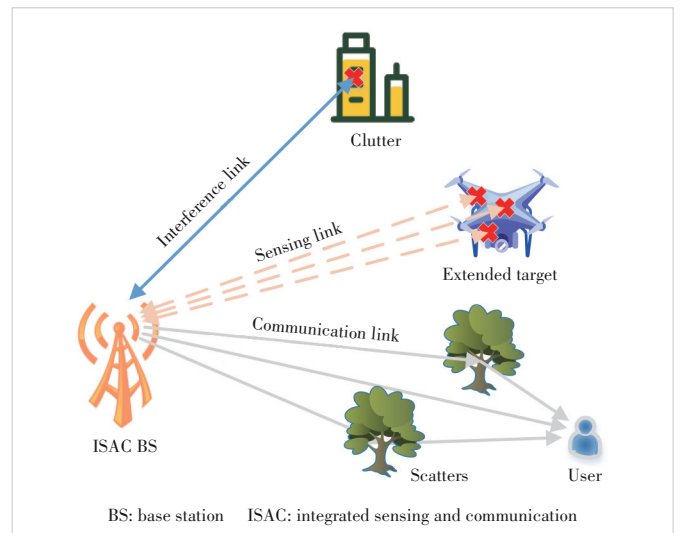
tion (SCA) method is used for constellation design, and the fractional optimization technique is employed for beamforming design. Simulation results reveal the tradeoff in terms of sensing, communication KLD, and the SINR of echo signals and BER in ISAC systems, validating that the proposed beamforming design can suppress the clutter and enhance sensing performance.

2 ISAC System Model with Clutter

We present the ISAC system model in the presence of static clutter and employ the KLD as a criterion to define a unified performance metric. This unified metric illustrates the relationship between KLD and demodulation error as well as detection probability.

2.1 System Model and Signal Model

As depicted in Fig. 1, we consider an ISAC system comprising one base station (BS), one single-antenna communication user, one sensing target, and static clutter. The ISAC BS is equipped with two uniform linear arrays (ULAs), each with M antennas. Besides serving the communication user, the BS also exploits the echoes of communication signals to detect the potential sensing target in a specific direction. Specifically, we denote the distance between the target and the BS as d_s , while the distance from BS to user is d_c . To enhance the realism of the model, the Saleh-Valenzuela channel model is considered for communication, comprising one line-of-sight (LoS) path and p non-LoS (NLoS) paths, and the extended target model is considered for sensing. Compared with the sensing target, the radar cross section (RCS) of scatters in communication links and users is much smaller, which is thus ignored in this paper. The angles of departure (AoD) for the LoS path and the p -th NLoS path of the BS-user link are denoted as θ_c and θ_p , respectively, while the AoD for the j -th sensing path is denoted as θ_j . Besides, the clutter is located at a distance of d_u



▲ Figure 1. An illustration of the considered ISAC system

from the BS in the direction of θ_u . Since the clutter is typically static, its AoD and distance information are assumed to be known at the BS, and a point model is employed to depict it. Besides, the clutter is passive and far away from the communication user, and therefore its impact on communication performance can be omitted.

With the ISAC waveform transmitted by the BS denoted as $\mathbf{s} = [s_1, \dots, s_L] \in \mathbb{C}^{1 \times L}$, where L denotes the number of snapshots, the discrete-time received signals $\mathbf{y}_c \in \mathbb{C}^{1 \times L}$ at the user can be expressed as

$$\mathbf{y}_c = \sqrt{\rho_0 d_c^{-2} P_t} \left(\mathbf{a}^H(\theta_c) + \sum_{p=1}^P \alpha_p \mathbf{a}^H(\theta_p) \right) \mathbf{w} \mathbf{s} + \mathbf{n}_c \triangleq \sqrt{\rho_0 d_c^{-2} P_t} \mathbf{h}_c \mathbf{w} \mathbf{s} + \mathbf{n}_c, \quad (1)$$

where ρ_0 denotes the path loss at the reference distance $d_0 = 1$ m, $\mathbf{a}(\theta) = [1, e^{j2\pi\delta \sin(\theta)}, \dots, e^{j2\pi(M-1)\delta \sin(\theta)}]^T \in \mathbb{C}^{M \times 1}$ is the transmit antenna steering vector with δ denoting the normalized antenna spacing, α_p denotes the small-scale fading of the p -th NLoS path, $\mathbf{w} \in \mathbb{C}^{M \times 1}$ denotes the normalized beamforming vector with $\mathbf{w}^H \mathbf{w} = 1$, and $\mathbf{n}_c \sim \mathcal{CN}(0, \sigma_c^2 \mathbf{I}_L)$ denotes the additive white Gaussian noise (AWGN) vector at the communication user.

As for sensing, the received sensing echo signals $\mathbf{Y}_r \in \mathbb{C}^{M \times L}$ at the BS can be expressed as:

$$\mathbf{Y}_r = \underbrace{\sqrt{\rho_0 d_t^{-4} P_t} \sum_{j=1}^J \mathbf{b}^*(\theta_j) \mathbf{a}^H(\theta_j) \mathbf{w} \mathbf{s}}_{\text{target component}} + \underbrace{\sqrt{\rho_0 d_u^{-4} P_t} \mathbf{b}^*(\theta_u) \mathbf{a}^H(\theta_u) \mathbf{w} \mathbf{s}}_{\text{clutter component}} + \underbrace{\mathbf{N}_r}_{\text{noise}}, \quad (2)$$

where $\mathbf{b}(\theta) \triangleq \mathbf{a}(\theta)$ denotes the receiving antenna steering vector, and $\mathbf{N}_r = [\mathbf{n}_{r,1}, \dots, \mathbf{n}_{r,L}]^T \in \mathbb{C}^{M \times L}$ denotes the AWGN at the BS with $\mathbf{n}_{r,l} \sim \mathcal{CN}(0, \sigma_r^2 \mathbf{I}_M), \forall 1 \leq l \leq L$. The detection of the potential target at the l -th frame can be cast as the binary hypothesis testing as follows:

$$\mathbf{y}_r = \begin{cases} \sqrt{\rho_0 d_u^{-4} P_t} \mathbf{b}^*(\theta_u) \mathbf{a}^H(\theta_u) \mathbf{w} \mathbf{s} + \mathbf{n}_r & \mathcal{H}_0 \\ \sqrt{\rho_0 d_t^{-4} P_t} \sum_{j=1}^J \mathbf{b}^*(\theta_j) \mathbf{a}^H(\theta_j) \mathbf{w} \mathbf{s} + \sqrt{\rho_0 d_u^{-4} P_t} \mathbf{b}^*(\theta_u) \mathbf{a}^H(\theta_u) \mathbf{w} \mathbf{s} + \mathbf{n}_r & \mathcal{H}_1 \end{cases}. \quad (3)$$

As evident from Eqs. (2) and (3), the existence of clutter can significantly affect the detection, indicating the necessity of clutter suppression.

2.2 KLD-Based Unified Performance Metric

For a pair of probability density functions (PDFs), KLD is defined as the relative entropy from one PDF $f_n(x)$ to another

PDF $f_m(x)$ to measure the information gain achieved by employing the distribution f_m instead of $f_n^{[13]}$, hence, the KLD can be defined as:

$$\text{KLD}_{n \rightarrow m} = \int_{-\infty}^{\infty} f_m(x) \log_2 \frac{f_m(x)}{f_n(x)} dx. \quad (4)$$

To compare the differences among multiple PDFs, one can consider the KLD between each pair of PDFs and take either the average or the minimum of all the comparison results. In communication systems, the KLD can be employed to assess the demodulation performance, as the error performance is significantly influenced by the pair of closest symbols. Specifically, for each pair of different data symbols $\{s_m, s_n\} (m \neq n)$ in a Q-ary signal constellation, the KLD in communication demodulation can be represented as:

$$\text{KLD}_c = \min_{n \neq m} \int_{-\infty}^{\infty} f_m(x) \log_2 \frac{f_m(x)}{f_n(x)} dx. \quad (5)$$

From the perspective of sensing systems, the KLD can be utilized to evaluate the difference between \mathcal{H}_0 and \mathcal{H}_1 , as Stein's Lemmas state that for any fixed false alarm probability, the maximization of the KLD between \mathcal{H}_0 and \mathcal{H}_1 leads to an asymptotic maximization of detection probability^[16], and hence, the KLD in sensing detection can be expressed as

$$\text{KLD}_r = \text{KLD}(\mathcal{H}_0 \| \mathcal{H}_1). \quad (6)$$

2.2.1 KLD for Communication

For communications, based on Eq. (1), the PDF of the received symbol y_c is given as

$$f_m(x) \triangleq f(y_c | \{s_m, \mathbf{w}\}) = \frac{\exp(-(\mathbf{y}_c - \boldsymbol{\mu}_m)^T \boldsymbol{\Sigma}^{-1} (\mathbf{y}_c - \boldsymbol{\mu}_m))}{\sqrt{(2\pi)^2 |\boldsymbol{\Sigma}_c|}}, \quad (7)$$

where $\mathbf{y}_c \triangleq [y_{c,R}, y_{c,I}]^T$ with $y_{c,R}$ and $y_{c,I}$ denoting the real and imaginary components of y_c , $\boldsymbol{\mu}_m \triangleq [\mu_{c,R}, \mu_{c,I}]^T$ with $\mu_{c,R} = \sqrt{\rho_0 d_c^{-2} P_t} \text{Re}\{\mathbf{h}_c \mathbf{w} s_m\}$ and $\mu_{c,I} = \sqrt{\rho_0 d_c^{-2} P_t} \text{Im}\{\mathbf{h}_c \mathbf{w} s_m\}$, and $\boldsymbol{\Sigma}_c = \sigma_c^2 \mathbf{I}_2$.

Substituting Eq. (7) into Eqs. (1) and (5), the KLD in communication can be expressed as

$$\text{KLD}_c = \min_{m \neq n} \frac{1}{2 \ln 2} \left(\text{tr}(\boldsymbol{\Sigma}_c^{-1} \boldsymbol{\Sigma}_c) - 2 + (\boldsymbol{\mu}_m - \boldsymbol{\mu}_n)^H \boldsymbol{\Sigma}_c^{-1} (\boldsymbol{\mu}_m - \boldsymbol{\mu}_n) + \ln \frac{|\boldsymbol{\Sigma}_c|}{|\boldsymbol{\Sigma}_c|} \right) = \min_{m \neq n} \frac{1}{2 \sigma_c^2 \ln 2} (\boldsymbol{\mu}_m - \boldsymbol{\mu}_n)^H (\boldsymbol{\mu}_m - \boldsymbol{\mu}_n). \quad (8)$$

It can be readily seen that an ISAC system with a larger

KLD_c value exhibits superior demodulation performance as corresponding transmit symbols mixed with noise can be more easily distinguished by the receiver.

2.2.2 KLD for Sensing

Based on Eq. (3), the PDFs of \mathbf{y}_r under \mathcal{H}_0 and \mathcal{H}_1 are expressed as:

$$\begin{aligned} f_0(\mathbf{y}_r) &= \frac{1}{\pi^M |\boldsymbol{\Sigma}_u|} \exp(-\mathbf{y}_r^H \boldsymbol{\Sigma}_u^{-1} \mathbf{y}_r), \\ f_1(\mathbf{y}_r) &= \frac{1}{\pi^M |\boldsymbol{\Sigma}_u + \boldsymbol{\Sigma}_s|} \exp(-\mathbf{y}_r^H (\boldsymbol{\Sigma}_u + \boldsymbol{\Sigma}_s)^{-1} \mathbf{y}_r), \end{aligned} \quad (9)$$

where $\boldsymbol{\Sigma}_s = \rho_0 d_t^{-4} P_t \mathbb{E}\{|s|^2\} \mathbf{A}_s \mathbf{W} \mathbf{A}_s^H$, $\mathbb{E}\{|s|^2\} = \sum_{m=1}^Q P_r(s_m) |s_m|^2$, $\mathbf{A}_s = \sum_{j=1}^J \mathbf{b}^s(\theta_j) \mathbf{a}^H(\theta_j)$, $\mathbf{W} = \mathbf{w} \mathbf{w}^H$ and $\boldsymbol{\Sigma}_u = \rho_0 d_t^{-4} P_t \mathbb{E}\{|s|^2\} \mathbf{A}_u \mathbf{W} \mathbf{A}_u^H + \sigma_r^2 \mathbf{I}_M$, $\mathbf{A}_u = \mathbf{b}^*(\theta_u) \mathbf{a}^H(\theta_u)$.

By substituting Eq. (9) into Eqs. (1) and (6), the KLD for target detection can be derived as

$$\begin{aligned} \text{KLD}_r &= \ln \left| \mathbf{I}_M + \boldsymbol{\Sigma}_u^{-1/2} \boldsymbol{\Sigma}_s \boldsymbol{\Sigma}_u^{-1/2} \right| + \\ &\text{tr} \left((\mathbf{I}_M + \boldsymbol{\Sigma}_u^{-1/2} \boldsymbol{\Sigma}_s \boldsymbol{\Sigma}_u^{-1/2})^{-1} - \mathbf{I}_M \right). \end{aligned} \quad (10)$$

The waveform design for detection can be addressed by maximizing KLD_r in Eq. (10) in order to obtain the optimal detection probability performance in terms of Stein's Lemmas^[16].

3 ISAC Constellation Design Under KLD Performance Metric

We investigate the methodology of constellation design under the KLD metrics in Eqs. (8) and (10) to achieve a tradeoff between sensing and communication performance in this section. Additionally, the maximum instantaneous transmit power constraint is considered to ensure the transmit power remains within the linear dynamic range of the amplifier.

The constellation design can be formulated as a max-min optimization problem with power constraints, which can be solved by the SCA algorithm. It's worth noting that the optimization of constellation reveals the inherent trade-off between sensing and communication performance.

3.1 Constellation Design Under Single-Antenna Setup

Based on the expressions in Eqs. (8) and (10), it is evident that the KLD performance metric is influenced by both the constellation set and the beamforming vector. In practice, the constellation set is fixed and shared between the transmitter and the receiver to minimize signaling overhead. Therefore, constellation design can be analyzed in a single-antenna setup, allowing for a separation of the constellation design from the beamforming design.

First, based on the KLD performance metrics in Eqs. (8) and (10), while ensuring the amplitude of the transmit symbol remains within the linear dynamic range of the amplifier, the ISAC constellation design problem can be formulated as

$$\begin{aligned} \max_{\{s_m\}} \text{KLD}_c \\ \text{s.t. } \text{KLD}_r \geq \text{KLD}_{r,\text{thresh.}} \\ |s_m|^2 \leq 1, m = 1, 2, \dots, Q, \end{aligned} \quad (11)$$

where $\text{KLD}_{r,\text{thresh.}}$ denotes the lower boundary of KLD_r in order to ensure the sensing performance.

To decouple the constellation design from the beamforming design, we consider a single-antenna scenario setup while substituting the expressions of the intermediate variables, and the KLD for communication in Eq. (8) can be simplified as follows.

$$\begin{aligned} \text{KLD}_c &= \min_{m \neq n} \frac{1}{2\sigma_c^2 \ln 2} (\boldsymbol{\mu}_m - \boldsymbol{\mu}_n)^H (\boldsymbol{\mu}_m - \boldsymbol{\mu}_n) = \\ &\frac{\rho_0 d_c^{-2} P_t}{2\sigma_c^2 \ln 2} \min_{m \neq n} |s_m - s_n|^2. \end{aligned} \quad (12)$$

We can see from Eq. (12) that the minimum distance among the inner points in the constellation determines the communication demodulation performance. This result makes sense as the minimum distance dictates the noise margin of the constellation.

Similarly, for a single-antenna scenario setup, the KLD for radar sensing in Eq. (10) can be simplified as^[17]:

$$\text{KLD}_r = \ln \left(1 + \frac{\zeta}{\sigma_r^2} \right) + \frac{\sigma_r^2}{\zeta + \sigma_r^2} - 1, \quad (13)$$

where $\zeta = \mathbb{E}\{|s_m|^2\} \rho_0 d_t^{-4} P_t$ denotes the power of echo signals. It can be readily seen from Eq. (12) that the KLD for sensing is positively related to $\mathbb{E}\{|s_m|^2\}$ as $f'(x) = 1/(1+x) - 1/(1+x)^2$ is always greater than 0 when $x > 0$ and KLD_r can be reformulated as $f(\mathbb{E}\{|s_m|^2\} \rho_0 d_t^{-4} P_t / \sigma_r^2)$, indicating the average power of inner points in the constellation determines the sensing performance.

Based on Eqs. (12) and (13), Problem (11) can be reformulated as

$$\begin{aligned} \max_{\{s_m\}} \min_{m \neq n} |s_m - s_n|^2 \\ \text{s.t. } r^2 \leq |s_m|^2 \leq 1, m = 1, 2, \dots, Q, \end{aligned} \quad (14)$$

where r constraints the average power of the constellation to ensure the difference between the echo signals and noise in the detection. The setting of r is intended to ensure the lower bound of the sensing performance of the ISAC system.

Problem (14) is non-convex and to address this, we utilize the SCA technique in the following discussion^[18].

3.2 Constellation Design with SCA

For ease of description and intuitive understanding, Problem (14) can be reformulated as

$$\begin{aligned} & \max_{\mathbf{S}} t \\ & \text{s.t. } r^2 \leq |s_m|^2 \leq 1, m = 1, 2, \dots, Q, \\ & |s_m - s_n|^2 \geq t^2, m, n = 1, 2, \dots, Q; m \neq n, \end{aligned} \quad (15)$$

where $\mathbf{S} = [s_1, \dots, s_Q] \in \mathbb{R}^{Q \times 2}$ with $s_i = [\text{Re}(s_i), \text{Im}(s_i)]^T$ denotes the point location in the constellation.

By introducing superscripts (l) to represent the value of variables at the l -th iteration and applying a first-order Taylor expansion to the constraints at $\mathbf{S}^{(l)}$, Problem (15) can be approximated as

$$\begin{aligned} & \max_{\Delta \mathbf{S}^{(l)}} t^{(l)} \\ & \text{s.t. } s_m^{(l)T} s_m^{(l)} + 2s_m^{(l)T} \Delta s_m^{(l)} + \Delta s_m^{(l)T} \Delta s_m^{(l)} \leq 1, m = 1, 2, \dots, Q \\ & s_m^{(l)T} s_m^{(l)} + 2s_m^{(l)T} \Delta s_m^{(l)} \geq r^2, m = 1, 2, \dots, Q \\ & s_m^{(l)T} s_m^{(l)} + s_n^{(l)T} s_n^{(l)} - 2s_m^{(l)T} s_n^{(l)} + \\ & 2(s_m^{(l)T} - s_n^{(l)T})(\Delta s_m^{(l)} - \Delta s_n^{(l)}) \geq t^{(l)}, \\ & m, n = 1, 2, \dots, Q; m \neq n \\ & t^{(l)} \geq t^{(l-1)}, \end{aligned} \quad (16)$$

where the second and third constraints are first-order Taylor approximations of the original expressions and the fourth is employed to ensure the minimum distance among inner points can continually increase with each iteration. By utilizing the optimal solution $\Delta \mathbf{S}_{\text{opt}}^{(l)}$ to update the original term with $\mathbf{S}^{(l+1)} = \mathbf{S}^{(l)} + \Delta \mathbf{S}_{\text{opt}}^{(l)}$ and repeatedly solving Problem (16) until it converges, we can eventually obtain \mathbf{S}^* .

The complexity of the constellation design mainly comes from the application of interior within each iteration, which is $O(I \times \ln(1/\varepsilon)Q^3)$, where I denotes the number of iterations, Q denotes the order of constellation and ε denotes the duality gap of the interior point method^[19]. It can be seen that the complexity of this algorithm primarily increases cubically with the dimension of variables.

As for the convergence of this algorithm, within each iteration, we have

$$\begin{aligned} & s_m^{(l)T} s_m^{(l)} + s_n^{(l)T} s_n^{(l)} - 2s_m^{(l)T} s_n^{(l)} + 2(s_m^{(l)T} - s_n^{(l)T})(\Delta s_m^{(l)} - \\ & \Delta s_n^{(l)}) \geq t^{(l)} \geq t^{(l-1)}, m, n = 1, 2, \dots, Q; m \neq n. \end{aligned} \quad (17)$$

The right side of Problem (17) shows that the value of objective function monotonically increases during the SCA process. Based on the first constraint in Problems (16) and (17), we have

$$\begin{aligned} t^{(l)} & \leq s_m^{(l)T} s_m^{(l)} + s_n^{(l)T} s_n^{(l)} - 2s_m^{(l)T} s_n^{(l)} + 2(s_m^{(l)T} - s_n^{(l)T})(\Delta s_m^{(l)} - \Delta s_n^{(l)}) = \\ & (s_m^{(l)T} s_m^{(l)} + 2s_m^{(l)T} \Delta s_m^{(l)} + (s_n^{(l)T} s_n^{(l)} + 2s_n^{(l)T} \Delta s_n^{(l)}) - \\ & 2(s_m^{(l)T} s_n^{(l)} + s_m^{(l)T} \Delta s_n^{(l)} + s_n^{(l)T} \Delta s_m^{(l)}) < \\ & 2 - 2(s_m^{(l)T} s_n^{(l)} + s_m^{(l)T} \Delta s_n^{(l)} + s_n^{(l)T} \Delta s_m^{(l)}) < \\ & 2 + 2(|s_m^{(l)}| |s_n^{(l)}| + |s_m^{(l)}| |\Delta s_n^{(l)}| + |s_n^{(l)}| |\Delta s_m^{(l)}|) = b_u. \end{aligned} \quad (18)$$

Note that the value of b_u is limited; hence, the alternating optimization is guaranteed to converge.

By setting different values of r , we can obtain the corresponding constellation to achieve various tradeoffs between sensing and communication performance as a larger r represents a higher average power for better detection, which also results in a smaller inner-constellation distance and poorer communication performance.

4 Sensing Clutter Suppression Design Based on KLD

In this section, we study the beamforming design in the presence of clutter as depicted in Fig. 1 with a fixed constellation set designed in Section 3. The aim of beamforming focuses more on clutter suppression, as the tradeoff between sensing and communication performance is adjusted by setting different values of r in the constellation design. We will show that the maximization of KLD in terms of sensing in the presence of clutter is eventually equivalent to maximizing the SINR of echo signals.

With the fixed constellation mapping designed in the previous section, the BS can achieve various tradeoffs between sensing and communication performance by setting different inner radii r in Problem (14). However, as indicated by Eq. (2), the influence of clutter still exists. To address this issue, we explore optimal beamforming to mitigate the impact of clutter based on Eq. (10) shown as follows.

In the presence of clutter, the KLD for sensing in Eq. (10) can be further derived as:

$$\begin{aligned} \text{KLD}_r & = \ln \left| (\boldsymbol{\Sigma}_u + \boldsymbol{\Sigma}_s) \boldsymbol{\Sigma}_s^{-1} \right| + \text{tr} \left[(\boldsymbol{\Sigma}_u + \boldsymbol{\Sigma}_s)^{-1} \boldsymbol{\Sigma}_s \right] = \\ & \ln \left| \mathbf{I}_M + \beta_s \mathbf{A}_s \mathbf{W} \mathbf{A}_s^H (\beta_u \mathbf{A}_u \mathbf{W} \mathbf{A}_u^H + \mathbf{I}_M)^{-1} \right| + \\ & \text{tr} \left[(\mathbf{I}_M + \beta_u \mathbf{A}_u \mathbf{W} \mathbf{A}_u^H)^{-1} \beta_s \mathbf{A}_s \mathbf{W} \mathbf{A}_s^H + \mathbf{I}_M \right]^{-1}, \end{aligned} \quad (19)$$

$$\text{where } \beta_s = \frac{\rho_0 d_s^{-4} P_t \mathbb{E} \left\{ |s_m|^2 \right\}}{\sigma_r^2} \text{ and } \beta_u = \frac{\rho_0 d_u^{-4} P_t \mathbb{E} \left\{ |s_m|^2 \right\}}{\sigma_r^2}.$$

In the following, we employ the KLD for sensing in the presence of clutter in Eq. (10) to explore the optimal beampattern to achieve clutter suppression. To further simplify KLD, we apply the Woodbury identity as follows^[20].

$$(\mathbf{A} + \mathbf{UCV})^{-1} = \mathbf{A}^{-1} - \mathbf{A}^{-1} \mathbf{U} (\mathbf{C}^{-1} + \mathbf{V} \mathbf{A}^{-1} \mathbf{U})^{-1} \mathbf{V} \mathbf{A}^{-1}, \quad (20)$$

where $\mathbf{A} \in \mathbb{C}^{M \times M}$, $\mathbf{U} \in \mathbb{C}^{M \times K}$, $\mathbf{C} \in \mathbb{C}^{K \times K}$ and $\mathbf{V} \in \mathbb{C}^{K \times M}$. By re-

placing matrices \mathbf{A} and \mathbf{C} with identity matrices, we can obtain

$$(\mathbf{I} + \mathbf{UV})^{-1} = \mathbf{I} - \mathbf{U}(\mathbf{I} + \mathbf{VU})^{-1}\mathbf{V}. \quad (21)$$

Then, let $\mathbf{U} = (\beta_u \mathbf{A}_u \mathbf{W} \mathbf{A}_u^H + \mathbf{I}_M)^{-1} \mathbf{A}_s \mathbf{w}$ and $\mathbf{V} = \beta_s \mathbf{w}^H \mathbf{A}_s^H$, we can obtain:

$$\text{KLD}_r = \ln \left(1 + \beta_s \mathbf{w}^H \mathbf{A}_s^H (\beta_u \mathbf{A}_u \mathbf{w} \mathbf{w}^H \mathbf{A}_u^H + \mathbf{I}_M)^{-1} \mathbf{A}_s \mathbf{w} \right) + \frac{1}{1 + \beta_s \mathbf{w}^H \mathbf{A}_s^H (\beta_u \mathbf{A}_u \mathbf{w} \mathbf{w}^H \mathbf{A}_u^H + \mathbf{I}_M)^{-1} \mathbf{A}_s \mathbf{w}}. \quad (22)$$

Again, note that $f(x) = \ln(1+x) + 1/(1+x)$ is monotonically increasing with the increase of x ; hence, the maximization of KLD_r can be formulated as:

$$\begin{aligned} \max_{\mathbf{w}} \quad & \beta_s \mathbf{w}^H \mathbf{A}_s^H (\beta_u \mathbf{A}_u \mathbf{w} \mathbf{w}^H \mathbf{A}_u^H + \mathbf{I}_M)^{-1} \mathbf{A}_s \mathbf{w} \\ \text{s.t.} \quad & \mathbf{w}^H \mathbf{w} = 1. \end{aligned} \quad (23)$$

It can be seen that the objective function of Problem (23) can be further transformed as follows.

$$\begin{aligned} & \beta_s \mathbf{w}^H \mathbf{A}_s^H (\beta_u \mathbf{A}_u \mathbf{w} \mathbf{w}^H \mathbf{A}_u^H + \mathbf{I}_M)^{-1} \mathbf{A}_s \mathbf{w} = \\ & \beta_s \mathbf{w}^H \mathbf{A}_s^H \mathbf{A}_s \mathbf{w} \operatorname{tr} \left[(\beta_u \mathbf{A}_u \mathbf{w} \mathbf{w}^H \mathbf{A}_u^H + \mathbf{I}_M)^{-1} \right] = \\ & \frac{\beta_s \mathbf{w}^H \mathbf{A}_s^H \mathbf{A}_s \mathbf{w}}{1 + \beta_u \mathbf{w}^H \mathbf{A}_u^H \mathbf{A}_u \mathbf{w}}. \end{aligned} \quad (24)$$

Based on the above results, Problem (23) can be reformulated as follows.

$$\begin{aligned} \max_{\mathbf{w}} \quad & \frac{\beta_s \mathbf{w}^H \mathbf{A}_s^H \mathbf{A}_s \mathbf{w}}{1 + \beta_u \mathbf{w}^H \mathbf{A}_u^H \mathbf{A}_u \mathbf{w}} \\ \text{s.t.} \quad & \mathbf{w}^H \mathbf{w} = 1. \end{aligned} \quad (25)$$

It can be observed that the KLD maximizing problem is eventually transformed to maximizing the SINR of echo signals, thereby achieving clutter suppression. To obtain the optimal beamforming vector of Problem (25), we first apply the constraint to transform the objective function of Problem (25) into

$$\frac{\beta_s \mathbf{w}^H \mathbf{A}_s^H \mathbf{A}_s \mathbf{w}}{1 + \beta_u \mathbf{w}^H \mathbf{A}_u^H \mathbf{A}_u \mathbf{w}} = \frac{\beta_s \mathbf{w}^H \mathbf{A}_s^H \mathbf{A}_s \mathbf{w}}{\beta_u \mathbf{w}^H (\frac{1}{\beta_u} \mathbf{I} + \mathbf{A}_u^H \mathbf{A}_u) \mathbf{w}}. \quad (26)$$

Since $\frac{1}{\beta_u} \mathbf{I} + \mathbf{A}_u^H \mathbf{A}_u$ is a positive semi-definite matrix, we consider its lower triangular Cholesky decomposition, i. e., $\mathbf{C}\mathbf{C}^H = \frac{1}{\beta_u} \mathbf{I} + \mathbf{A}_u^H \mathbf{A}_u$. Let $\mathbf{w} = (\mathbf{C}^H)^{-1} \mathbf{y}$, and we can obtain:

$$\frac{\beta_s \mathbf{w}^H \mathbf{A}_s^H \mathbf{A}_s \mathbf{w}}{\beta_u \mathbf{w}^H (\frac{1}{\beta_u} \mathbf{I} + \mathbf{A}_u^H \mathbf{A}_u) \mathbf{w}} = \frac{\beta_s \mathbf{y}^H \mathbf{C}^{-1} \mathbf{A}_s^H \mathbf{A}_s (\mathbf{C}^H)^{-1} \mathbf{y}}{\beta_u \mathbf{y}^H \mathbf{y}}. \quad (27)$$

According to the Rayleigh quotient^[21], Problem (25) has a closed-form solution as shown below.

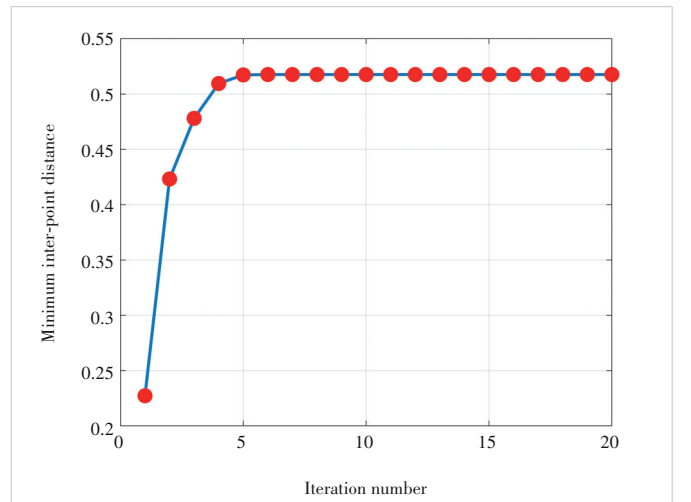
$$\mathbf{w}^* = \frac{(\mathbf{C}^H)^{-1} \mathbf{u}_{\max}}{\|(\mathbf{C}^H)^{-1} \mathbf{u}_{\max}\|}, \quad (28)$$

where \mathbf{u}_{\max} denotes the eigenvector of $\mathbf{C}^{-1} \mathbf{A}_s^H \mathbf{A}_s (\mathbf{C}^H)^{-1}$ corresponding to the largest eigenvalue λ_{\max} . By utilizing the optimal transmit beamforming vector in Eq. (25), the BS can effectively suppress clutter by maximizing the SINR of the echo signals, as demonstrated in Problem (25), which leads to enhanced sensing performance in the ISAC system.

5 Numerical Results

In this section, we provide numerical results to demonstrate the performance of the constellation and beamforming design methodology. The number of antennas is set as $M = 16$ and the inner-element spacing is $\lambda/2$ with λ denoting the wavelength of the transmit signal. The transmit power of BS is set as 30 dBm and the path loss at the reference distance of 1 m is set as -30 dBm. In addition, the DoAs of the target, user and static clutter are $\theta_s = 30^\circ$, $\theta_c = 18^\circ$ and $\theta_u = 45^\circ$, respectively. Besides, the BS-target, the BS-user and the BS-clutter distances are set as $d_s = 600$ m, $d_c = 800$ m and $d_u = 750$ m. The noise power at the BS and the user is set as -110 dBm and -70 dBm, respectively. The number of NLoS links is set as 4 while the number of scattering points on the extended target is set as 10.

The convergence behavior of the SCA algorithm for constellation design is shown in Fig. 2, illustrating the minimum inter-point distance t versus the iteration number for $Q = 16$ and $r = 0.4$. It is shown that the minimum inter-point distance stabilizes by the fourth iteration, indicating that the algorithm has converged. This demonstrates the good convergence of



▲ Figure 2. Minimum inter-point distance versus iteration number

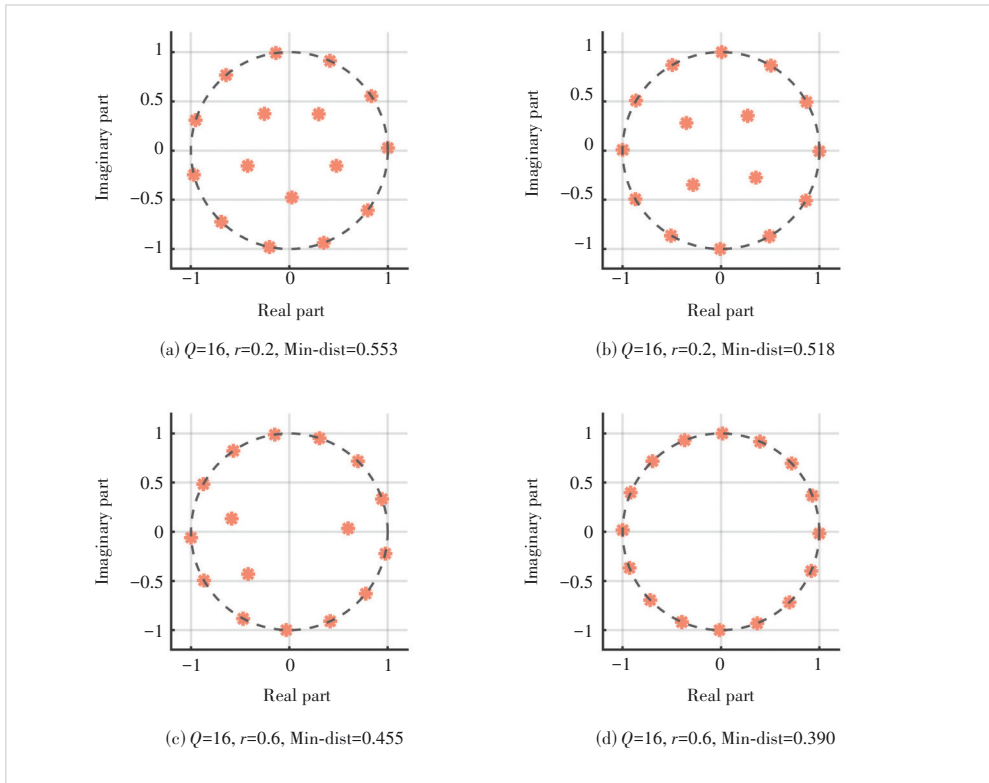
this SCA algorithm for constellation design algorithm.

Next, in Fig. 3, we provide the optimized constellation set with various inner ring radii r and the modulation order of $Q = 16$. A larger r results in a smaller minimum inter-point distance within the constellation. This results in more constellation points clustering at the edge of the unit circle, leading to a gradual transition of the constellation mapping from irregular to regular. This demonstrates tuning r can generate different constellations and the corresponding result can achieve different tradeoffs between sensing and communication performance.

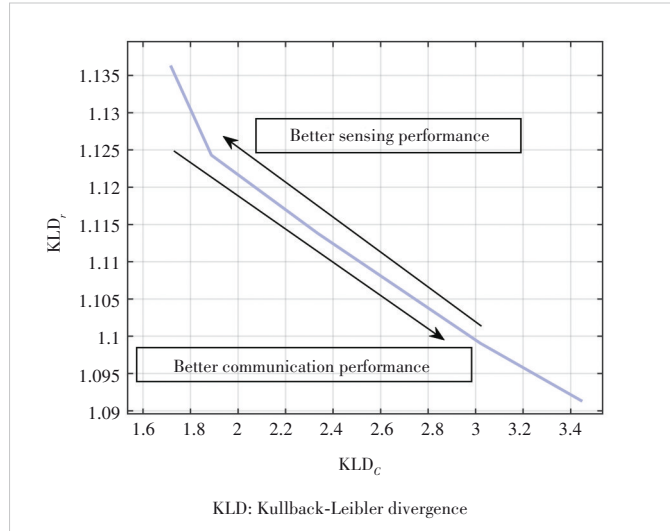
To further investigate the performance tradeoff, we illustrate the Pareto bound between sensing and communication from the perspective of KLD in Fig. 4. The constellations designed in Fig. 3 are taken into consideration. It can be seen that KLD_r strictly and monotonically decreases with the increase of KLD_c , indicating an inherent tradeoff in the ISAC system. With higher inner ring radii r , more constellation points cluster at the edge of the unit circle, shifting the tradeoff state from right bottom to left top in Fig. 4 and vice versa. Therefore, we can achieve the desired performance tradeoff to meet various needs by selecting corresponding constellations.

As a step further, we evaluate the performance of the transmit beampattern generated by the proposed design methodology compared with the beampattern generated by the Maximum Ratio Transmission (MRT) algorithm and the methods proposed in Ref. [14], as shown in Fig. 5. The beampattern generated by the MRT algorithm exhibits significant power gain in the direction of targets while the beampattern from Ref. [14] has high gain in both the direction of the user and the target as the ISAC system design in Ref. [14] considers the tradeoff between sensing and communication through beamforming. However, the influence of static clutter is overlooked in these schemes. In contrast, the transmitted waveform generated by our proposed algorithm is predominantly focused in the desired direction, while a deep fading occurs in the clutter direction. This indicates that the proposed scheme effectively achieves clutter suppression, thereby enhancing overall sensing performance.

In Fig. 6, we further evaluate the performance of the pro-

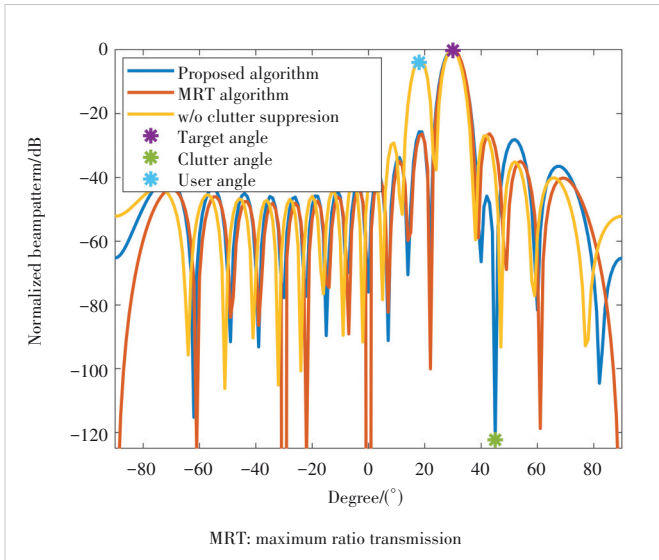


▲ Figure 3. Constellation under different inner ring radii r

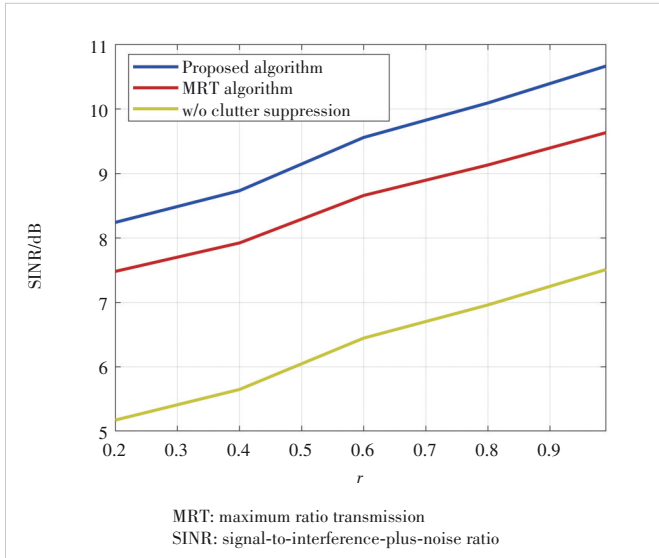


▲ Figure 4. Tradeoff between sensing and communication

posed design by comparing the SINR of echo signals with other algorithms. The optimized ISAC constellation under various r is employed in this example. As it can be seen, the proposed algorithm achieves 0.7 dB gain over the MRT algorithm and 3 dB gain over the method in Ref. [14], indicating the proposed algorithm can successfully achieve clutter suppression better. The method in Ref. [14] allocates more power to the user direction but less power to the target direction to balance



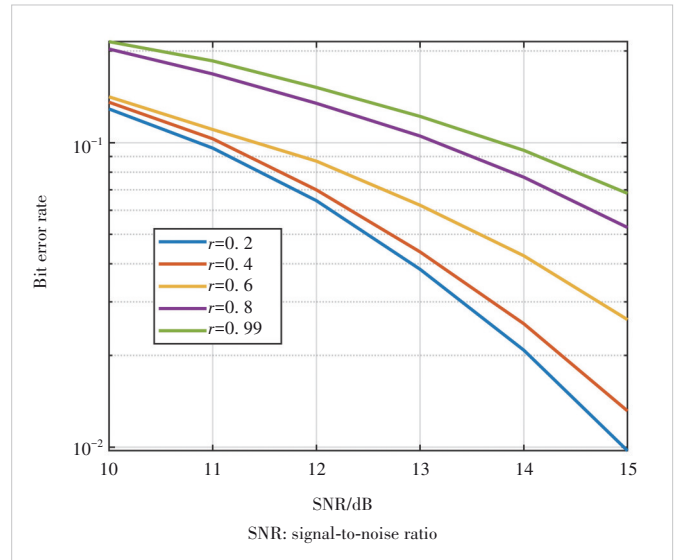
▲ Figure 5. Transmit beampattern comparison



▲ Figure 6. SINR of echo signals versus inner ring radii r

sensing and communication as depicted in Fig. 5. Consequently, the SINR is the lowest in comparison. Besides, regardless of the algorithm employed, the SINR is monotonically increasing with the increase of r . This is attributed to the greater clustering of constellation points along the edge of the unit circle, resulting in an overall increase in the average power of the corresponding constellation.

With the transmit beampattern generated by the proposed design methodology, we further evaluate the BER performance of various constellation mappings under different r . As illustrated in Fig. 7, a better demodulation performance is achieved by a smaller r as constellation points with lower power are more likely to be distributed within the unit circle, resulting in a larger inter-point distance. Considering Figs. 5 and 6, the tradeoff between communication and sensing perfor-



▲ Figure 7. Bit error rate versus SNR under different inner ring radii r

mance in the ISAC system stems from the balance between randomness and determinism, while the value of r is required to be set according to realistic requirements.

6 Conclusions

In this paper, we investigated a comprehensive design methodology for constellation and beamforming in ISAC systems, particularly in environments with static clutter. We utilized the KLD as a critical metric in our analysis. Initially, we introduced a unified ISAC performance metric based on KLD and used this metric to guide the ISAC constellation design through the SCA technique. Following this, we demonstrated that the optimal beamforming design, guided by KLD, is mathematically equivalent to maximizing the SINR of echo signals. We derived a closed-form solution from this beamforming strategy. Simulation results validated the effectiveness of our proposed constellation design methodology and clutter suppression technology, clearly illustrating the inherent performance tradeoffs in ISAC systems. In future work, we will consider more complex real-world scenarios, including more intricate clutter distributions and the influence of strong scatters in communication links. The deeper performance tradeoff in ISAC systems will be investigated in our future work.

References

- [1] LIU F, ZHENG L, CUI Y H, et al. Seventy years of radar and communications: the road from separation to integration [J]. IEEE signal processing magazine, 2023, 40(5): 106 – 121. DOI: 10.1109/MSP.2023.3272881
- [2] LIANG H, LIAO B. Robust hybrid beamforming for MIMO-ISAC system with CSI imperfection [C]//The 6th International Conference on Information Communication and Signal Processing (ICICSP). IEEE, 2023: 665 – 669. DOI: 10.1109/ICICSP59554.2023.10390724
- [3] CHEN W J, DENG Y L, GUO C T, et al. Transmit beampattern optimization for MIMO-ISAC systems with hybrid beamforming [C]//The IEEE In-

- ternational Conference on Acoustics, Speech and Signal Processing (ICASSP). IEEE, 2024: 8651 - 8655. DOI: 10.1109/ICASSP48485.2024.10447252
- [4] LIU R, LI M, LIU Q, et al. Dual-functional radar-communication waveform design: a symbol-level precoding approach [J]. IEEE journal of selected topics in signal processing, 2021, 15(6): 1316 - 1331. DOI: 10.1109/JSTSP.2021.3111438
- [5] ZHANG Y, QI H T, LU W D, et al. Beamforming design for IRS-assisted OFDM-ISAC system in C-RAN [J]. IEEE wireless communications letters, 2024, 13(6): 1626 - 1630. DOI: 10.1109/LWC.2024.3384249
- [6] LIU W X, XU H B, HE X L, et al. Bi-level deep unfolding based robust beamforming design for IRS-assisted ISAC system [J]. IEEE access, 2024, 12: 76663 - 76672. DOI: 10.1109/ACCESS.2024.3406527
- [7] ZHAO Z Y, ZHANG L, JIANG R, et al. Joint beamforming scheme for ISAC systems via robust Cramér-Rao bound optimization [J]. IEEE wireless communications letters, 2024, 13(3): 889 - 893. DOI: 10.1109/LWC.2024.3349488
- [8] WANG X Y, FEI Z S, HUANG J X, et al. Joint waveform and discrete phase shift design for RIS-assisted integrated sensing and communication system under cramer-Rao bound constraint [J]. IEEE transactions on vehicular technology, 2022, 71(1): 1004 - 1009. DOI: 10.1109/TVT.2021.3122889
- [9] FUHRMANN D R, SAN ANTONIO G. Transmit beamforming for MIMO radar systems using signal cross-correlation [J]. IEEE transactions on aerospace and electronic systems, 2008, 44(1): 171 - 186. DOI: 10.1109/TAES.2008.4516997
- [10] TANG B, NAGHSH M M, TANG J. Relative entropy-based waveform design for MIMO radar detection in the presence of clutter and interference [J]. IEEE transactions on signal processing, 2015, 63(14): 3783 - 3796. DOI: 10.1109/TSP.2015.2423257
- [11] LI J, ZHOU G, GONG T T, et al. A framework for mutual information-based MIMO integrated sensing and communication beamforming design [J]. IEEE transactions on vehicular technology, 2024, 73(6): 8352 - 8366. DOI: 10.1109/TVT.2024.3355899
- [12] PIAO J H, WEI Z Q, YUAN X, et al. Mutual information metrics for up-link MIMO-OFDM integrated sensing and communication system [C]// IEEE Global Communications Conference. IEEE, 2023: 7387 - 7392. DOI: 10.1109/GLOBECOM54140.2023.10437900
- [13] AL-JARRAH M, ALSUSA E, MASOUROS C. A unified performance framework for integrated sensing-communications based on KL-divergence [J]. IEEE transactions on wireless communications, 2023, 22(12): 9390 - 9411. DOI: 10.1109/TWC.2023.3270390
- [14] FEI Z, TANG S, WANG X, et al. Revealing the trade-off in ISAC systems: the KL divergence perspective [J]. IEEE wireless communications letters, 2024, 13(10): 2747 - 2751. DOI: 10.1109/LWC.2024.3443409
- [15] KLOOB Y, AL-JARRAH M, ALSUSA E, et al. Novel KLD-based resource allocation for integrated sensing and communication [J]. IEEE transactions on signal processing, 2024, 72: 2292 - 2307. DOI: 10.1109/TSP.2024.3392350
- [16] KAILATH T. The divergence and bhattacharyya distance measures in signal selection [J]. IEEE transactions on communication technology, 1967, 15(1): 52 - 60. DOI: 10.1109/TCOM.1967.1089532
- [17] WANG X Y, FEI Z S, LIU P, et al. Sensing aided covert communications: turning interference into allies [J]. IEEE transactions on wireless communications, 2024, PP(99): 1. DOI: 10.1109/TWC.2024.3374775
- [18] JEANNE R S, SAMUNDISWARY P. Power minimization in MIMO-OFDM network with energy harvesting node using Successive Convex Approximation (SCA) technique [C]//Proceedings of International Conference on Control, Instrumentation, Communication and Computational Technologies (ICCICT). IEEE, 2016: 431 - 436. DOI: 10.1109/ICCICT.2016.7987988
- [19] WALDSPURGER I, D' ASPREMONTE A, MALLAT S. Phase recovery, MaxCut and complex semidefinite programming [J]. Mathematical programming, 2015, 149(1): 47 - 81. DOI: 10.1007/s10107-013-0738-9
- [20] BUDHU J, GRBIC A. Accelerated optimization of metasurfaces with the Woodbury matrix identity [C]//International Applied Computational Electromagnetics Society Symposium (ACES). IEEE, 2021: 1 - 3
- [21] SUN J G. Eigenvalues of Rayleigh quotient matrices [J]. Numerische mathematik, 1991, 59(1): 603 - 614. DOI: 10.1007/BF01385798

Biographies

TANG Shuntian received his BE degree in electronic engineering from Beijing Institute of Technology (BIT), China in 2024. He is currently pursuing his master's degree with BIT. His research interests include integrated sensing and communications and AFDM modulation.

WANG Xinyi (bit_wangxy@163.com) received his BE and PhD degrees in electronic engineering from Beijing Institute of Technology (BIT), China in 2017 and 2022, respectively. He is currently a postdoctoral researcher at BIT. He was a recipient of the Best Paper Award in WOCC 2019 and has been recognized as an exemplary reviewer for the *IEEE Transactions on Communications*. His research interests include integrated sensing and communications, UAV communications, intelligent reflecting surface, polar codes, and OTFS modulation. He has published over 50 journals and conference papers in these areas.

XIA Fanghao received his BS degree in electronic engineering from Beijing Institute of Technology (BIT), China in 2021. He is currently pursuing his PhD degree with the Research Institute of Communication Technology, BIT. His research interests include integrated sensing and communications, intelligent reflection surface, and physical layer security.

FEI Zesong received his PhD degree in electronic engineering from Beijing Institute of Technology (BIT), China in 2004. He is currently a professor with the Research Institute of Communication Technology, BIT, where he is involved in the design of the next generation high-speed wireless communication. He is the chief investigator with the National Natural Science Foundation of China. His research interests include wireless communications and multimedia signal processing. He is a senior member of the Chinese Institute of Electronics and China Institute of Communications.